RSC Advances

PAPER

View Article Online
View Journal | View Issue

Check for updates

Cite this: *RSC Adv.*, 2019, **9**, 4599

Ionic association analysis of LiTDI, LiFSI and $LiPF_6$ in EC/DMC for better Li-ion battery performances

Christopher L. Berhaut, *[ac] Daniel Lemordant, [a] Patrice Porion, [b] Laure Timperman, [a] Grégory Schmidt[c] and Mériem Anouti [a]

New lithium salts such as lithium bis(fluorosulfonyl)imide (LiFSI) and lithium 4,5-dicyano-2-(trifluoromethyl) imidazole-1-ide (LiTDI) are now challenging lithium hexafluorophosphate ($LiPF_6$), the most used electrolyte salt in commercial Li-ion batteries. Thus it is now important to establish a comparison of these electrolyte components in a standard solvent mixture of ethylene carbonate and dimethyl carbonate (EC/DMC: 50/50 wt%). With this aim, transport properties, such as the ionic conductivity, viscosity and ^{7}Li self-diffusion coefficient have been deeply investigated. Moreover, as these properties are directly linked to the nature of the interionic interactions and ion solvation, a better understanding of the structural properties of electrolytes can be obtained. The Li salt concentration has been varied over the range of 0.1 mol L^{-1} to 2 mol L^{-1} at 25 °C and the working temperature from 20 °C to 80 °C at the fixed concentration of 1 mol L^{-1}. Experimental results were used to investigate the temperature dependence of the salt ion-pair (IP) dissociation coefficient (α_D) with the help of the Walden rule and the Nernst–Einstein equation. The lithium cation effective solute radius (r_{Li}) has been determined using the Jones–Dole–Kaminsky equation coupled to the Einstein relation for the viscosity of hard spheres in solution and the Stokes–Einstein equation. From the variations of α_D and r_{Li} with the temperature, it is inferred that in EC/DMC LiFSI forms solvent-shared ion-pairs (SIP) and that, LiTDI and $LiPF_6$ are likely to form solvent separated ion-pairs (S_2IP) or a mixture of SIP and S_2IP. From the temperature dependence of α_D, thermodynamic parameters such as the standard Gibbs free energy, enthalpy and entropy for the ion-pair formation are obtained. Besides being in agreement with the information provided by the variations of α_D and r_{Li}, it is concluded that the ion-pair formation process is exergonic and endothermic for the three salts in EC/DMC.

Received 11th October 2018
Accepted 28th January 2019

DOI: 10.1039/c8ra08430k

rsc.li/rsc-advances

Open Access Article. Published on 06 febrero 2019. Downloaded on 14/08/2025 20:05:26.
This article is licensed under a Creative Commons Attribution-NonCommercial 3.0 Unported Licence.

1. Introduction

The current desire to continuously increase the use of renewable and green energy in order to reduce the dependence on fossil fuel reserves comes with the necessity to multiply solar, tidal and wind power harvesting technologies. However, green energy is intermittent and depends on the weather. An energy shortage (at night, during windless and/or cloudless periods) has as much chance of happening as an energy surplus (summer days, storms). The use of technologies capable of storing energy directly where it is produced does not only solve the problem of the uncertainty of green energy delivery but also relieves the power grid and prevents its expansion. Indeed, the produced energy does not have to be transported over great distances as it is when coming from large-scale power plants, and the line-losses are reduced. Batteries are ideal candidates for such an application. Furthermore, stationary batteries can buffer voltage fluctuations to meet the power demands of consumers.

The lithium-ion battery (LiB) is the most popular rechargeable battery compared to other technologies due to its high energy density and its good cycle life.[1–6] Since the commercialization of its first generation by Sony in 1990 (ref. 7) LiBs have known an impressive increase in performance and a decrease in price.[8] Today, LiBs can not only be found in all kinds of portable electronic devices such as smartphones, portable computers and digital cameras but also in larger systems such as electric vehicles.[6] Thus, because of the increasing use of the LiB technology it is important for the future LiB generations to be even more performant and safe. To increase the energy density of LiBs higher-capacity materials are being explored. Oxygen-based and sulfur (Li_2S) positive electrodes are currently being studied[9,10] while silicon-alloys[11–13] show promising results as negative electrode material. Safety can be improved through a better choice of the battery components.

The electrolyte is one of the most important component of Li-ion batteries and represented a production of 103 kt and 1.4 B$ in revenues in 2016.[14] Among all the Li salts that can be used

[a]*Laboratoire PCM2E (EA 6296), Université François Rabelais de Tours, UFR Sciences et Techniques, Parc de Grandmont, 37200 Tours, France. E-mail: christopher.berhaut@outlook.com*

[b]*ICMN CNRS - Université d'Orléans, UMR 7374, 1b rue de la Férollerie, 45071 Orléans Cedex 02, France*

[c]*ARKEMA, rue Henri Moissan, 69493 Pierre Bénite, France*

Open Access Article. Published on 06 febrero 2019. Downloaded on 14/08/2025 20:05:26.
This article is licensed under a Creative Commons Attribution-NonCommercial 3.0 Unported Licence.

as electrolyte salts, only lithium tetrafluoroborate ($LiBF_4$) and lithium hexafluorophosphate ($LiPF_6$) have been commercialized in current cells. Nevertheless, new salts like lithium bis(-fluorosulfonyl)imide (LiFSI) and lithium 4,5-dicyano-2-(trifluoromethyl)imidazole-1-ide (LiTDI) are now challenging $LiPF_6$. Despite exhibiting many advantages over $LiPF_6$, the main limitation for their use in commercial batteries is their cost and availability. One of the objectives of this article is to establish a comparison between $LiPF_6$, LiTDI and LiFSI dissolved in a standard solvent: a mixture of ethylene carbonate and dimethyl carbonate (EC/DMC: 50/50 wt%). Beside security issues and interface stability with electrode materials, ion transport properties are the most important features for an electrolyte. Hence, in this work is presented an extended comparative study of the electrolyte transport properties, such as ion conductivity, electrolyte viscosity and self-diffusion coefficients. Moreover, from a deep study of these properties, are inferred other important parameters such as ion size, ion solvation and ion pairing, which can allow a better understanding of the behavior of lithium salts in solution.[15,16]

2. Theory

2.1. Ion-pairing

Electrolytes for Li-ion batteries generally contain 1 mol L^{-1} of lithium salt dissolved in a mixture of alkylcarbonate solvents such as EC/DMC. In spite of the relatively high dielectric constant of EC, the formation of ion-pairs (IP) may occur. If M^+, X^- and S stand respectively for the metallic cation, the anion and a solvent molecule then three kinds of ion-pairs are commonly described as illustrated in Fig. 1: (M^+X^-) the contact ion-pairs (CIP), (M^+SX^-) the solvent shared ion-pairs (SIP) and the (M^+SSX^-) solvent separated ion-pairs (S_2IP) when both ions retain their primary solvation shell. In low permittivity solvents higher ion-aggregates (AGG) may exist such as $M^+X^-M^+$ triple ions, $(M^+X^-)_2$ ion-pair dimers, or even larger species.[17,18] Ion-pair population varies with ion size, solvent properties and temperature. The thermodynamic parameters describing ion association are the molar Gibbs free energy (ΔG_{IP}) for ion pairing and the related enthalpy (ΔH_{IP}) and entropy (ΔS_{IP}). These parameters are linked to each other and to the activity ratio (Q_r) and equilibrium constant (K_{IP}) of the chemical reaction describing the association, by the following equation.

$$\Delta G_{IP} = \Delta H_{IP} - T\Delta S_{IP} = RT \ln(Q_r/K_{IP}) \quad (1)$$

The ionic association process which leads to CIP or SIP is generally dominated by a positive ΔH_{IP}.

$$\Delta H_{IP} = \Delta H_{el} + \Delta H_{sol} \quad (2)$$

where ΔH_{el} and ΔH_{sol} are the electric and solvation contributions to enthalpy.

The coulombic energy released when two oppositely charged ions are brought together, forming an ion pair, is an exothermic process ($\Delta H_{el} < 0$ J mol^{-1}) but this contribution is overcompensated by the de-solvation contribution making the ion-pairing enthalpy $\Delta H_{IP}(T)$ positive. As a matter of fact, during association, the electric field becomes smaller around the ions that are now paired and consequently, an appreciable number of electrostricted solvent molecules are released to the bulk solvent. This phenomenon, being the inverse process of solvation, leads to a large endothermic solvation enthalpy contribution (ΔH_{sol}) which dominates the overall enthalpy ΔH_{IP}. The entropy variation ΔS_{IP} corresponding to the formation of an ion pair can also be expressed as the sum of two terms:

$$\Delta S_{IP} = \Delta S + \Delta S_{sol} \quad (3)$$

where ΔS and ΔS_{sol} are respectively the ion pairing entropy variation under vacuum and the entropy variation resulting from the change in ion solvation in the considered solvent.

Ion association leads to a decrease in entropy $\Delta S < 0$ J K^{-1} mol^{-1} as a solution containing un-associated ions is more disordered than a solution containing ion-pairs. Still, the displacement of solvent molecules from the solvation shell of the cation or the anion to the bulk solvent leads to a positive contribution ($\Delta S_{sol} > 0$ J K^{-1} mol^{-1}) to the global entropy. The sign of ΔS_{IP} depends on the magnitude of these two opposite contributions. Often the resulting ion pairing entropy is positive.

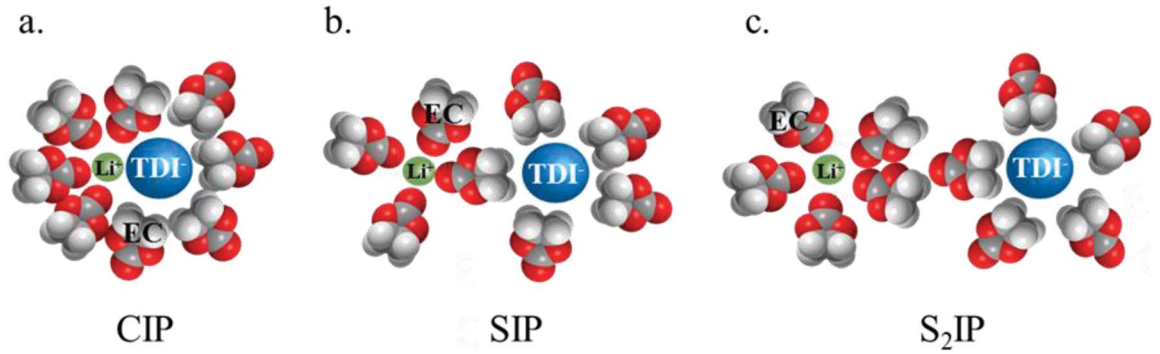

Fig. 1 Schematic view of different types of ion-pairs, (a) contact ion-pair (CIP), (b) solvent-shared ion-pair (SIP) and (c) solvent separated ion-pair (S_2IP) in the case of the LiTDI salt dissolved in EC.

This journal is © The Royal Society of Chemistry 2019

Open Access Article. Published on 06 febrero 2019. Downloaded on 14/08/2025 20:05:26.
This article is licensed under a Creative Commons Attribution-NonCommercial 3.0 Unported Licence.

In the case of CIP and SIP, a large release of solvating molecules to the bulk occurs and hence $\Delta H_{IP} \geq 0$ J mol^{-1} and $\Delta S_{IP} > 0$ J K^{-1} mol^{-1}. According to the Van't Hoff equation, any increase in temperature will favors ion pairing. On the contrary, in the case of S_2IP only solvent molecules belonging to the second solvation shell may be released during ion-pairing leading to a low and possibly negative association enthalpy and entropy. In consequence, any temperature increase will have no effect or favor ion-pair dissociation, depending on the magnitude of ΔH_{IP}.

2.2. Lithium effective ionic radius

As presented in Fig. 2, the Li^+ effective solute radius (r_s) represents the radius of the sphere englobing the species that participate in the first solvation layer of the lithium cation, its center.

Two methods were used herein to estimate r_s. The first one makes use of the Stokes–Einstein equation applied to ^{7}Li self-diffusion coefficients as:

$$D(\mathrm{Li}) = kT/c \quad (4)$$

where c and k are the drag coefficient and the Boltzmann constant. For spherical entities, the drag coefficient is related to the effective radius $r_{s,stokes}$ by applying the Stokes law:

$$c = 6\pi\eta r_{s,stokes} \quad (5)$$

where η is the viscosity of the electrolyte. Thus, from eqn (4) and (5) the effective Stokes radius can be deduced:

$$r_{s,stokes} = (kT)/(6\pi\eta D(\mathrm{Li})) \quad (6)$$

The second approach for determining r_s, is to use both the Einstein relation for the viscosity of a solution of hard spheres and its extension to spherical shaped suspensions (8)[19] and the Jones–Dole–Kaminsky (JDK) eqn (7):[20–23]

$$\eta_r = 1 + A\sqrt{C} + BC + DC^2 \quad (7)$$

In this equation, η_r is the relative viscosity of the solution ($\eta_r = \eta/\eta^\circ$), C the salt concentration and A, B, D parameters describing respectively long-range ion–ion interactions, volume effects and short-range interactions. At concentrations higher than 0.1 mol L^{-1} the $A\sqrt{C}$ term is negligible.[24] The B parameter is closely linked to the molar volume of the solute as indicated by the Einstein relation (8). Finally, D remains an adjustable parameter as no equation has yet been found to calculate this term. At concentrations lower than 0.1 mol L^{-1} the DC^2 term can be considered negligible compared to the other terms of the JDK equation but is predominant at higher concentrations.

$$B = 2.5\left[\frac{4}{3}\pi r_{s,JDK}{}^3 N_A\right] \quad (8)$$

where B is the JDK equation parameter, N_A the Avogadro number (6.022×10^{23} mol^{-1}) and $r_{s,JDK}$ the solute effective radius determined by using the JDK equation. Hence, its value is given by:

$$r_{s,JDK} = \sqrt[3]{\frac{3}{10\pi N_A}B} \quad (9)$$

2.3. Ion-pair dissociation coefficients

The dissociation coefficient (α_D) of the lithium salt, dissolved at the concentration C in the solvent mixture, is defined by the equilibrium described in Fig. 3.

Determining α_D is not straightforward when the solute activity coefficient is difficult to determine and this is the case for the present electrolytes.

Nevertheless, two alternative methods can be used for this purpose. The first one makes use of the Walden rule (Method 1) and the second involves the use of the self-diffusion coefficients of the charged species (Method 2).

2.3.1. Method 1: the Walden rule. The classical Walden rule[25] is an empirical rule stating that the molar conductivity Λ (mS cm^2 mol^{-1}) times the viscosity η (mPa s) is constant for the same ionic species in different solvents. However, the $\Lambda\eta$ product independence to the solvent is only true at high dilution at which point ionic association is negligible and salt concentration does not affect viscosity.[26] This rule is relatively well adapted to the study of aqueous solutions and of a high number of organic solutions. Angell has extended the previous relation to other types of solutions by introducing the "fractional Walden rule"[27] (10):

$$\Lambda\eta^\nu = \text{constant} \quad (10)$$

where ν is a constant $0 < \nu < 1$.[28–31]

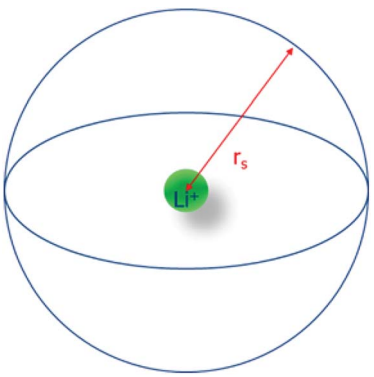

Fig. 2 Schema presenting the lithium cation effective solute radius.

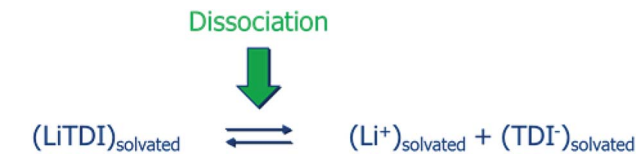

Fig. 3 Schema defining the dissociation phenomena.

Open Access Article. Published on 06 febrero 2019. Downloaded on 14/08/2025 20:05:26.
This article is licensed under a Creative Commons Attribution-NonCommercial 3.0 Unported Licence.

Table 1 Values of the constant ν of the fractional Walden rule for LiTDI,[32] $LiPF_6$ (ref. 32) and LiFSI

	LiTDI	$LiPF_6$	LiFSI
ν	1.0	0.9	0.8

By plotting $\ln(\Lambda)$ *vs.* $\ln(\eta)$ for the present electrolytes, ν was found to be close to 1 as indicated by the values displayed in Table 1.

The dissociation coefficients of LiTDI, $LiPF_6$ and LiFSI could then be estimated using eqn (11):[33–35]

$$\frac{\Lambda^{\exp}\,\eta}{\Lambda^{\circ}\,\eta^{\circ}} = \alpha_{\mathrm{D,\,Wal}} \tag{11}$$

where $\Lambda^{\exp}$, $\Lambda^{\circ}(T)$ and $\eta^{\circ}(T)$ are the measured molar conductivity, the high dilution limiting molar conductivity (reported in Table 2) and the solvent viscosity, all three depending on the temperature.

The limiting molar conductivity Λ° values were obtained by extrapolating at high dilution the variations of Λ *vs.* $C^{1/2}$ according to the Debye–Hückel–Onsager eqn (12):

$$\Lambda^{\exp} = \Lambda^{\circ} - S\sqrt[2]{C} \tag{12}$$

where S is a constant.

2.3.2. Method 2: Nernst–Einstein equation. This method involves the knowledge of the self-diffusion coefficient values of the ionic species.[36] The ratio of the experimental molar conductivity $\Lambda^{\exp}$ to the molar conductivity (S m^2 mol^{-1}) calculated from the Nernst–Einstein equation (Λ^{NE}) represents the dissociation coefficient of the considered salt:

$$\alpha_{\mathrm{D,\,NE}} = \frac{\Lambda^{\exp}}{\Lambda^{\mathrm{NE}}} \tag{13}$$

Λ^{NE} is calculated using eqn (14):

$$\Lambda^{\mathrm{NE}} = \frac{F^2}{RT}(D^+ + D^-) \tag{14}$$

where F is the Faraday constant, R the ideal gas constant, D^+ and D^- the self-diffusion coefficients of the cation and the anion, and T the temperature. The measured self-diffusion coefficients of the lithiated species ($D(^7Li)$) and of the fluorinated species ($D(^{19}F)$) were considered close enough to D^+ and D^- to consider that:

$$\Lambda^{\mathrm{NE}} = \frac{F^2}{RT}(D(^7\mathrm{Li}) + D(^{19}\mathrm{F})) \tag{15}$$

Table 2 Limiting molar conductivity Λ° values of LiTDI, LiFSI, and $LiPF_6$ in EC/DMC (50/50 wt%) at different temperatures

		25 °C	50 °C	60 °C	80 °C
Λ° (10^{-4} × S m^2 mol^{-1})	LiTDI	50.5	68.9	76.6	92.2
	LiFSI	43.5	59.2	65.5	78.8
	$LiPF_6$	49.4	63.7	79.4	85.7

Λ^{NE} values are derived from the assumption that all of the diffusing lithiated and fluorinated species detected during the Pulse-Gradient Spin-Echo Nuclear Magnetic Resonance (PGSE-NMR) measurement contribute to the molar conductivity. Hence, the Nernst–Einstein equation gives the molar conductivity of the electrolyte as it should be if all ion-pairs were dissociated and/or if all charged species contribute to the bulk conductivity.

3. Experimental

3.1. Material and cell preparation

Highly pure (GC grade, molecular purity >99%) ethylene carbonate (EC) purchased from Fluka, and anhydrous dimethylcarbonate (DMC, molecular purity >99%) purchased from Sigma-Aldrich, were used as received. The alkyl-carbonate EC/DMC (50/50 wt%) mixture used was prepared using a Sartorius 1602 MP balance with a $\pm 1 \times 10^{-4}$ g accuracy in an argon filled MBraun glove box at 25 °C with less than 5 ppm of moister content. A GeneCust desiccant bag was placed in the mixture to reduce the water content to a minimal level.

The battery grade lithium hexafluorophosphate ($LiPF_6$) purchased from Fluorochem was kept and used under the dry atmosphere of the glove box.

The lithium 4,5-dicyano-2-(trifluoromethyl)imidazole-1-ide (LiTDI) and lithium bis(fluorosulfonyl)imide (LiFSI) were supplied by Arkema (Pierre-Bénite, France). Before use LiTDI was dried under vacuum at 120 °C and then placed under a dry atmosphere in the glove box and kept there. LiTDI, LiFSI and $LiPF_6$ were dissolved in EC/DMC (50/50 wt%) at concentrations going from 1×10^{-4} mol L^{-1} to 2 mol L^{-1} in the glove box and kept there until use.

Prior to any measurement, the water content of each electrolyte was measured using an 831 Karl-Fisher Coulometer (Metrohm). The water content of the $LiPF_6$ and LiFSI electrolytes was lower than 20 ± 1 ppm and that of the LiTDI electrolytes, lower than 100 ± 1 ppm as this salt is very hygroscopic.

3.2. Experimental methods

3.2.1. Conductivity measurements. Were performed using two different instruments. The first is a Crison (GLP 31) digital multi-frequencies (1000–5000 Hz) conductometer. The temperature (from 10 °C to 80 °C) was controlled by a JULABO thermostat bath with an accuracy of 0.2 °C. Before any measurement the conductometer cell was calibrated using standard KCl solutions at three different concentrations. The second instrument is a BioLogic Multichannel Conductivity Meter based on frequency Response Analyser (MCM 10) connected to a Peltier based temperature control unit with 10 slots (WTSH 10). The measurements where made using sealed cells with Pt parallel plate electrodes protecting the samples from air exposure.

3.2.2. Density and viscosity measurements. Were carried out from 10 °C to 60 °C using respectively an Anton Parr digital vibrating tube densitometer (model 60/602, Anton Parr, France) and an Anton Parr rolling-ball viscometer (Lovis 2000M/ME,

 This journal is © The Royal Society of Chemistry 2019

Open Access Article. Published on 06 febrero 2019. Downloaded on 14/08/2025 20:05:26.
This article is licensed under a Creative Commons Attribution-NonCommercial 3.0 Unported Licence.

Anton Parr, France). In both cases the cell temperature was regulated within ±0.02 °C. Dynamic viscosity values reported in this paper were calculated by taking into account the effect of the sample density and the buoyancy of the ball in each sample as a function of temperature. The densitometer was firstly calibrated at all temperatures with degassed water and dehumidified air at atmospheric pressure as recommended by the constructor while ultra-pure water was used to calibrate the viscometer. The uncertainty of the density and viscosity measurements were better than 5×10^{-5} g cm^{-3}, and 1%, respectively.

3.2.3. Pulse-gradient spin-echo NMR (PGSE-NMR). Experiments were performed on a Bruker DSX100 NMR spectrometer with a 2.35 T superconducting magnet, equipped with a 10 mm microimaging probe (Micro5 Bruker) without a lock system. The Larmor resonance frequencies are 39.91 MHz and 94.20 MHz for ^{7}Li and ^{19}F nuclei, respectively. All measurements were performed with the same NMR pulse sequence. In order to determine the activation energy for the diffusion process of each species, the NMR runs were carried out over a temperature range from 20 °C to 80 °C within an accuracy of ±1 °C and a step $\Delta T = 5$ °C. The samples were prepared and placed in sealed glass tubes in a glove box. For NMR measurements, samples were thermally equilibrated at each temperature during 30 min before any acquisition in order to allow a good homogeneity of the set point temperature across the whole samples. Finally, all chemical shift references were set to a particular arbitrary value for convenience. Self-diffusion data concerning $LiPF_6$ and LiTDI in EC/DMC are taken from the literature.

4. Results and discussion

The transport properties of LiTDI, LiFSI and $LiPF_6$ in EC/DMC are investigated at fixed concentration (1 mol L^{-1}) over a large temperature range or at 25 °C as a function of the concentration in Li salt that ranges from 0 to 2 mol L^{-1}. From these results, the Li^+ effective radius, the mean ion-pair dissociation coefficient and the thermodynamic parameters for ion-pair formation are determined. Finally, the most likely ion-pair structure for these salts is proposed.

4.1. Conductivity, viscosity and self-diffusion coefficients

Conductivities and viscosities of the studied electrolytes are used here to calculate the ion-pair (IP) dissociation coefficient by using the Walden rule. With this aim, LiFSI conductivities and viscosities in EC/DMC have been measured as a function of the temperature and the results are presented in Fig. 4.

The data plotted in Fig. 4 shows that the Arrhenius equations for the conductivity and the viscosity are verified:

$$\eta = \eta_0 \exp \frac{1}{R}\left[\frac{E_{a_\eta}}{T}\right] \quad (16)$$

$$\sigma = \sigma_0 \exp \frac{1}{R}\left[\frac{-E_{a_\sigma}}{T}\right] \quad (17)$$

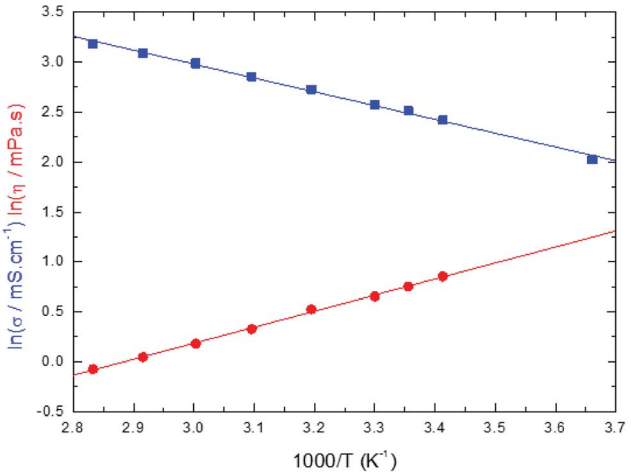

Fig. 4 Logarithmic plot of the conductivity (blue squares) and the viscosity (red discs) of LiFSI at 1 mol L^{-1} in EC/DMC (50/50 wt%) as a function of 1/T.

In eqn (16) and (17), E_{a_η} and E_{a_σ} are the activation energies for the two processes and η_0 and σ_0 fitting parameters. The values of these parameters are reported in Table 3 together with those for LiTDI and $LiPF_6$ in EC/DMC. The R^2 correlation coefficient values, which are over 0.99, show that eqn (16) and (17) fit perfectly the experimental results obtained over the temperature range investigated.

The E_{a_σ} values are a slightly lower than that of E_{a_η} but, by taking into account the uncertainty, it can be considered that $E_{a_\sigma} \simeq E_{a_\eta}$ (especially for LiTDI). When $E_{a_\sigma} = E_{a_\eta}$ the Walden product $\sigma\eta$ is strictly independent of the temperature and hence remains constant. Thus, this relation in only approximately verified.

Conductivity variations at 25 °C of LiTDI, LiFSI and $LiPF_6$ in EC/DMC have been represented as a function of the salt concentration in Fig. 5. All curves present a maximum of conductivity, which depends on the nature of the anion: at 0.75 mol L^{-1} for LiTDI, 1 mol L^{-1} for $LiPF_6$ and 1.16 mol L^{-1} for LiFSI. The maximum of conductivity σ_{max} for each electrolyte is reported in Table 4. In the case of LiTDI, σ_{max} is only of 6.8

Table 3 Arrhenius fitting parameters for the conductivity and viscosity of the investigated 1 mol L^{-1} LiX (X = TDI^-, FSI^- or PF_6^-) in EC/DMC (50/50 wt%) electrolytes with R^2 the correlation coefficient resulting from the fit procedure

Conductivity	σ_0 (mS cm^{-1})	E_{a_σ} (kJ mol^{-1}) ±0.5	R^2
LiTDI	1324	13.6	0.9948
LiFSI	1292	11.6	0.9965
$LiPF_6$	1545	12.1	0.9986
Viscosity	η_0	E_{a_η} (kJ mol^{-1}) ±0.5	R^2
LiTDI	0.017	14.1	0.9992
LiFSI	0.009	13.4	0.9979
$LiPF_6$	0.011	14.1	0.9984

Open Access Article. Published on 06 febrero 2019. Downloaded on 14/08/2025 20:05:26.
This article is licensed under a Creative Commons Attribution-NonCommercial 3.0 Unported Licence.

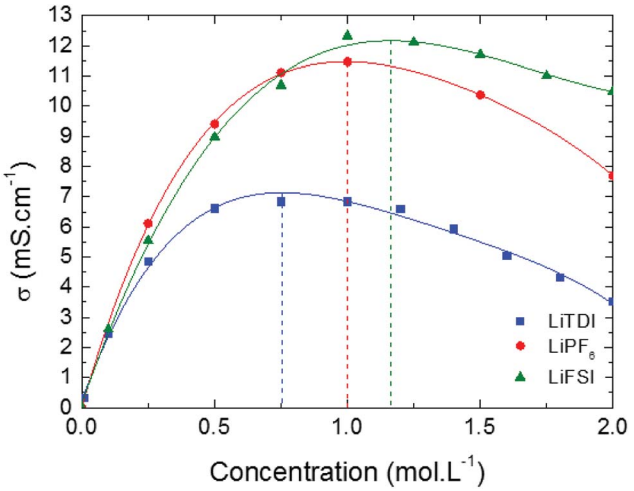

Fig. 5 Conductivity of LiTDI, LiFSI and $LiPF_6$ in EC/DMC at 25 °C as a function of the salt concentration.

Table 4 Maximum conductivity (σ_{max}) and concentration in salt at which it is obtained (C_m) in EC/DMC at 25 °C

	LiTDI	LiFSI	$LiPF_6$
σ_{max} (mS cm^{-1})	6.8	12.3	11.4
C_m (mol L^{-1})	0.75	1.16	1.00

mS cm^{-1} owing to its lower dissociation coefficient[32] in EC/DMC. This means that LiTDI starts forming ion-pairs at a lower concentration than LiFSI and $LiPF_6$. Once the maximum conductivity is reached, the conductivity drops more or less sharply owing to the increase in viscosity that depends on the salt anion.

The ^7Li and ^{19}F self-diffusion coefficients ($D(^7Li)$ and $D(^{19}F)$) of the LiTDI, $LiPF_6$ and LiFSI at 1 mol L^{-1} in EC/DMC electrolytes were determined by PGSE-NMR as a function of the temperature. Results are reported in Fig. 6.

It can be noticed that $D(^7Li)$, which corresponds to the self-diffusion of all species containing at least one ^7Li nucleus, does not exhibit any significate change from one lithium salt to the other contrarily to $D(^{19}F)$, the self-diffusion of all species containing at least one ^{19}F nucleus. $D(^{19}F)$ values are larger than $D(^7Li)$ and depends on the anion size with the following sequence:

$$D(^{19}F)_{TDI} < D(^{19}F)_{FSI} \simeq D(^{19}F)_{PF6}$$

Hence, the species containing a smaller anion diffuse more rapidly.

4.2. Lithium effective ionic radius

Relative viscosities of LiTDI and LiFSI in EC/DMC are plotted against the salt concentration in Fig. 7 at several temperatures. All curves have been fitted according to the JDK eqn (7). It can be noticed that the DC^2 term of this equation becomes predominant when the salt concentration is over 0.1 mol L^{-1}. The fitting curves exhibit a high correlation constant: $R^2 = 0.99999$, justifying the use of the JDK equation.

The JDK equation B parameter values and that of the $r_{s,JDK}$ radii, deduced from eqn (9), for the LiTDI, LiFSI and $LiPF_6$

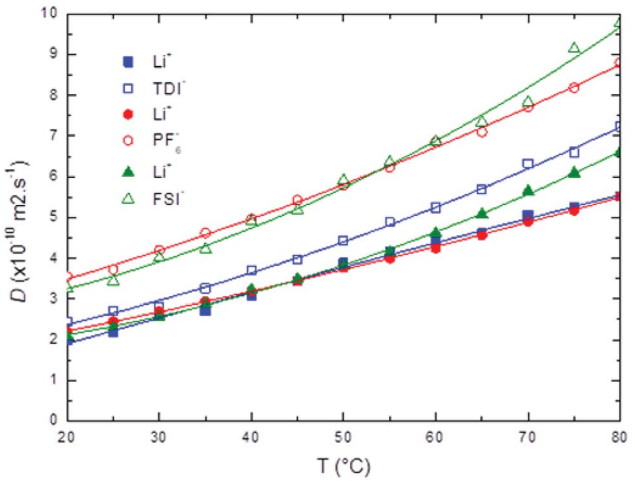

Fig. 6 ^7Li and ^{19}F self-diffusion coefficients ($D(^7Li)$ and $D(^{19}F)$) of LiTDI (blue squares), $LiPF_6$ (red circles) and LiFSI (green triangles) at 1 mol L^{-1} in EC/DMC as a function of the temperature.

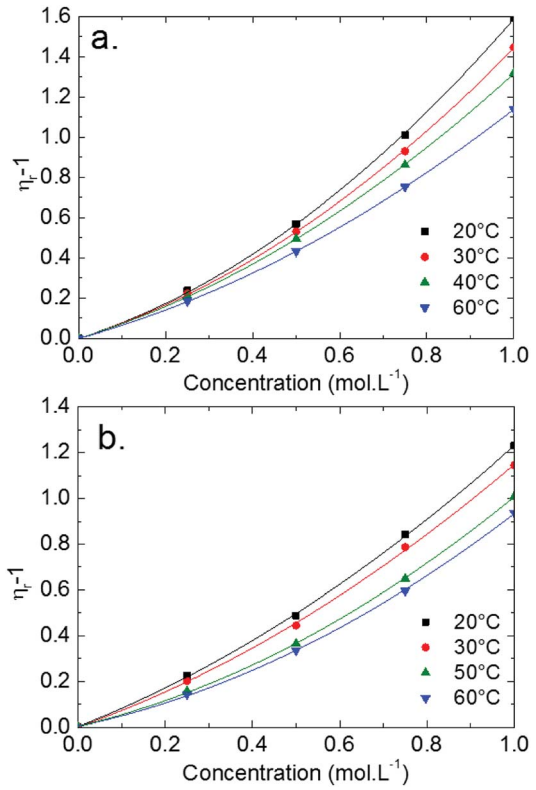

Fig. 7 Variations of the relative viscosity ($\eta_r - 1$) as a function of the concentration of LiTDI (a) and LiFSI (b) in EC/DMC at several temperatures.

This journal is © The Royal Society of Chemistry 2019

Open Access Article. Published on 06 febrero 2019. Downloaded on 14/08/2025 20:05:26.
This article is licensed under a Creative Commons Attribution-NonCommercial 3.0 Unported Licence.

Table 5 Values of B and of $r_{s,JDK}$ obtained by coupling the Einstein relation and the JDK equation for LiTDI, LiFSI and $LiPF_6$ in EC/DMC

	T (°C)	B (L mol^{-1})	$r_{s,JDK}$ (nm)
LiTDI	20	0.69	0.48
	30	0.68	0.48
	40	0.66	0.47
	60	0.66	0.48
LiFSI	20	0.75	0.49
	30	0.68	0.47
	50	0.45	0.42
	60	0.40	0.40
$LiPF_6$	20	0.43	0.41
	30	0.49	0.43
	40	0.55	0.45
	60	0.64	0.47

electrolytes are reported in Table 5. The Li^+ effective solute radius, which has been obtained by using the JDK equation coupled to the Einstein relation and by applying the Stokes–Einstein equation, is plotted against the temperature in Fig. 8.

The graphs reported in Fig. 8 show that $r_{s,JDK}$ values are systematically larger than $r_{s,Stokes}$. The reason for that is not clear but in the case of $r_{s,JDK}$, the ions or ion-pairs are submitted to a shear stress but not in the case of $r_{s,Stokes}$ which is deduced from self-diffusion measurements. Hence, the transport conditions are not strictly equivalent and the number of solvating molecules could be different.

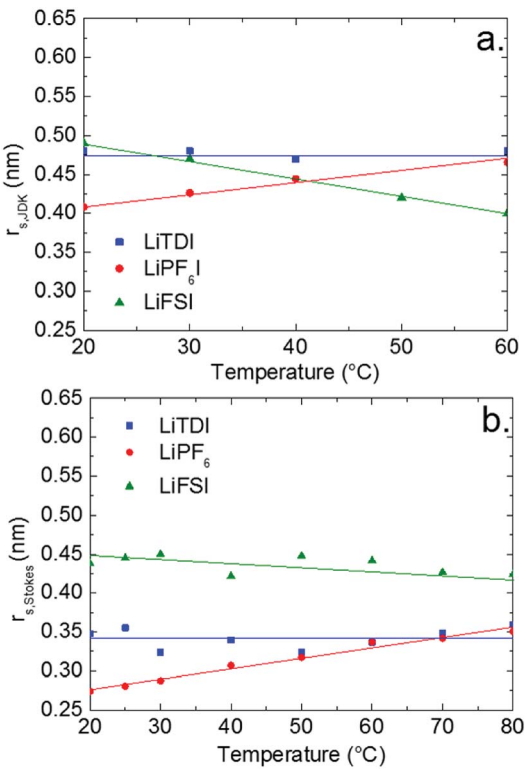

Fig. 8 The effective Li^+ solute radius calculated from the JDK equation (a) and the Stokes–Einstein equation (b) in the electrolytes containing 1 mol L^{-1} of LiTDI, LiFSI or $LiPF_6$ in EC/DMC as a function of the temperature.

Regarding the variations of $r_{s,JDK}$ and $r_{s\ Stokes}$ with the temperature, the same trend is observed when the temperature is increased: r_s (Li^+, LiTDI) does not vary significantly, r_s (Li^+, $LiPF_6$) increases and r_s (Li^+, LiFSI) decreases. This suggests that the three lithium salts form different types of ion-pairs which themselves exhibit a different behavior when the temperature is raised. This will be analyzed in the following paragraphs.

The first solvation layer of the lithium cation for LiTDI in EC/DMC has been modelized using the Conductor-Like Screening Model (COSMO) procedure. The results of this simulation are represented in Fig. 9. Three solvent molecules and one anion were arranged around the cation without considering polarization and deformation of the electron cloud.

The black circle having the lithium cation at its center corresponds to the section of the JDK solvation sphere (radius $r_{s,JDK}$). As the $r_{s,Stokes}$ is even smaller, it appears clearly that the JDK equation allows a better estimation of the lithium effective solute radius. One possible reason for that is that the $r_{s,Stokes}$ values are deduced from $D(^7Li)$, the self-diffusion coefficient of all species containing a lithium ion and not D^+, that of free lithium ions only.

4.3. Ion-pair dissociation coefficients

Variations of the ion-pair dissociation coefficients with the temperature which are obtained by using eqn (11) ($\alpha_{D,Wal}$) or eqn (13) ($\alpha_{D,NE}$) are plotted in Fig. 10.

As expected from its lower conductivity, LiTDI is the less dissociated salt of the three in EC/DMC even with TDI^-, a large hückel anion with a highly delocalized negative charge.[37] The size of the anion and its delocalized charge should be in favor of poor coulombic interactions. It can be noticed that both methods lead to α_D values which are in fair agreement for LiTDI and LiFSI but not for $LiPF_6$ as the difference reaches 15%. As indicated by the graphs reported in Fig. 10, both methods agree on the variations of α_D with the temperature: α_D does not depend on the temperature in the case of the LiTDI based electrolyte, but on the contrary, decreases with the temperature in the case of $LiPF_6$ and LiFSI. These observations suggest that the ion pairs formed by each salt in EC/DMC do not have the same structure. It can also be noted that the temperature

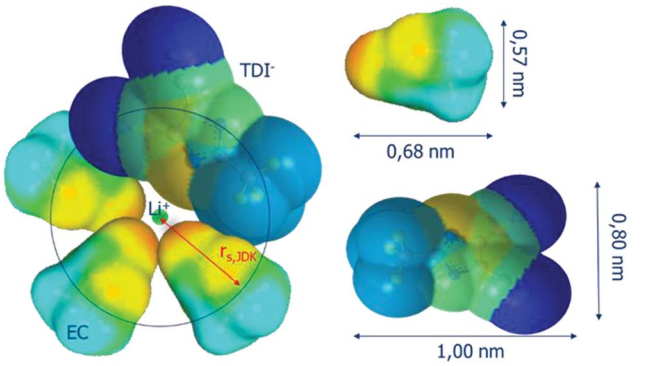

Fig. 9 Representation of the first solvation sphere of Li^+ in the case of LiTDI dissolved in EC/DMC.

Open Access Article. Published on 06 febrero 2019. Downloaded on 14/08/2025 20:05:26.
This article is licensed under a Creative Commons Attribution-NonCommercial 3.0 Unported Licence.

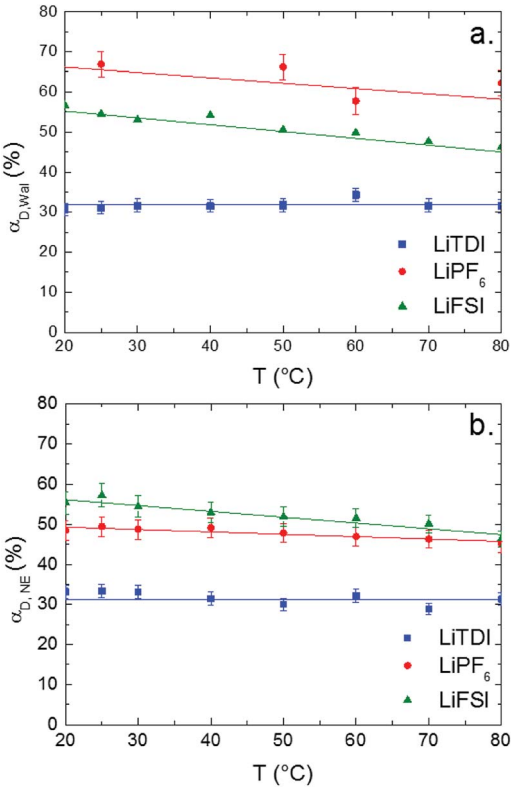

Fig. 10 Dissociation coefficients of LiTDI, LiFSI and $LiPF_6$ in EC/DMC at 1 mol L^{-1} measured using the Walden rule (a) and the Nernst–Einstein equation (b), as a function of the temperature.

independence of α_D (LiTDI) is in agreement with the relation between the activation energies $E_{a_\eta} \approx E_{a_\sigma}$ which has been found experimentally for LiTDI. Thus, according to eqn (16) and (17), the Walden product does not depend on the temperature.

4.4. Gibbs free energy of association for LiTDI, LiPF6 and LiFSI in EC/DMC

The dissociation coefficient of LiTDI, LiFSI and $LiPF_6$ in EC/DMC, which is strictly below 1 at the selected concentration of 1 mol L^{-1}, is evidence of the existence of ion-pairs and/or larger aggregates within the electrolytes. The equilibrium constant K_{IP} for ion pair formation:

$$Li^+ + X^- \rightarrow LiX$$

can be deduced from α_D values by:

$$K_{IP} = \frac{(1-\alpha_D)}{\alpha_D{}^2 C} \quad (18)$$

The standard Gibbs free energy for ion pair formation, ΔG°_{IP}, can be calculated by:

$$\Delta G^\circ_{IP} = -RT \ln(K_{IP}) \quad (19)$$

The temperature dependence of ΔG°_{IP} is plotted in Fig. 11. ΔG°_{IP} values calculated with $\alpha_{D,Wal}$ and $\alpha_{D,\,NE}$ are close excepted

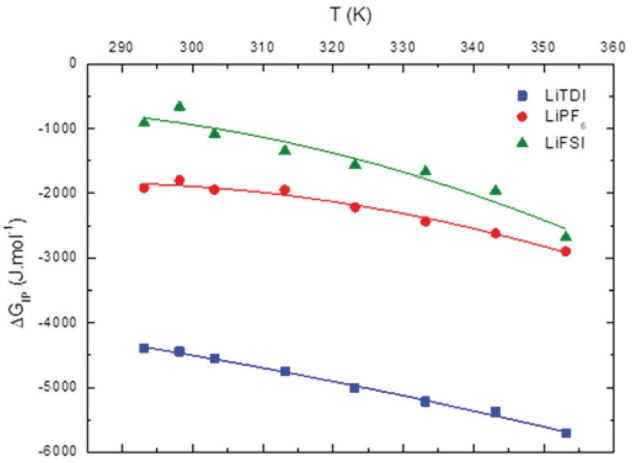

Fig. 11 Standard Gibbs free energy ΔG°_{IP} for ion pair formation as a function of the temperature for LiTDI, $LiPF_6$ and LiFSI at 1 mol L^{-1} in EC/DMC.

in the case of $LiPF_6$. Because the LiFSI-EC/DMC electrolyte has a higher conductivity than $LiPF_6$-EC/DMC it is likely that LiFSI is in a less associated state in the present experiment conditions. Thus, the considered ΔG°_{IP} ($LiPF_6$) was calculated using $\alpha_{D,NE}$.

For $LiPF_6$ and LiFSI in EC/DMC, ΔG°_{IP} values are negative. Thus, the entropy contribution to the free energy dominate the enthalpy contribution meaning that ion-pair formation here follows an exergonic process. ΔG°_{IP} decreases when the temperature rises owing to the weakening of ion–solvent interactions. That is also the case for LiTDI even though IP association was seen to be very weakly temperature dependent (Fig. 10). ΔG°_{IP} variations can be fitted by the following polynomial equation:[16]

$$\Delta G^\circ_{IP} = aT^2 + bT + c \quad (20)$$

Values of constants a, b and c are summarized in Table 6 along with the correlation coefficient R^2.

ΔH°_{IP} and ΔS°_{IP}, respectively the ion-pair formation standard enthalpy and entropy can be calculated by using eqn (21) and (22):

$$\Delta H^\circ_{IP} = \Delta G^\circ_{IP} + T\Delta S^\circ_{IP} \quad (21)$$

$$\Delta S^\circ_{IP} = -\left(\frac{\partial \Delta G^\circ_{IP}}{\partial T}\right)_P = -2aT - b \quad (22)$$

ΔH°_{IP} and ΔS°_{IP} variations with the temperature are presented in Fig. 12.

Table 6 Values of the a, b and c constants in eqn (20) for LiTDI, $LiPF_6$ and LiFSI at 1 mol L^{-1} in EC/DMC. R^2 is the correlation coefficient

	a (J mol^{-1} K^{-2})	b (J mol^{-1} K^{-1})	c (J mol^{-1})	R^2
LiTDI	−0.06	17.02	−4193	0.994
$LiPF_6$	−0.23	128.82	−20117	0.97
LiFSI	−0.25	135.16	−18685	0.92

This journal is © The Royal Society of Chemistry 2019

Open Access Article. Published on 06 febrero 2019. Downloaded on 14/08/2025 20:05:26.
This article is licensed under a Creative Commons Attribution-NonCommercial 3.0 Unported Licence.

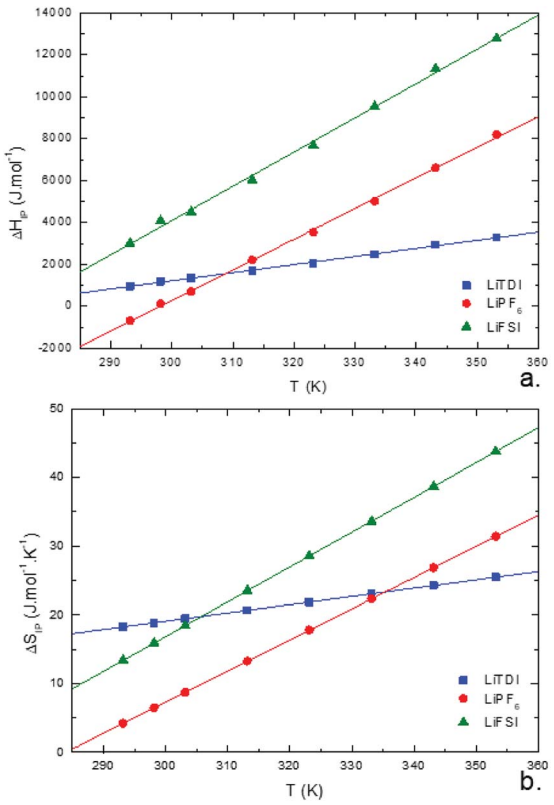

Fig. 12 Standard enthalpy ΔH°_{IP} (a) and entropy ΔS°_{IP} (b) for ion-pair formation as a function of the temperature for LiTDI, $LiPF_6$ and LiFSI at 1 mol L^{-1} in EC/DMC.

ΔH°_{IP} and ΔS°_{IP} values both increase with the temperature. ΔH°_{IP} is negative only for $LiPF_6$ below 300 K and ΔS°_{IP} is always positive. For these lithium salts in EC/DMC, ion-pairing is an endothermic process excepted for $LiPF_6$ at temperatures below 300 K.

Entropy can be taken as a measure of disorder resulting from the formation of ion-pairs. During the association process, the number of molecules is reduced from 2 to 1 which means that a change in ion solvation occurs: more than one solvent molecule is released and this number is likely to increase when the temperature is raised. However, increasing the electrolyte temperature has a low impact on the association entropy of the LiTDI-based electrolyte. This could be explained by considering that the kind of ion-pairs formed by LiTDI in EC/DMC are of the S_2IP type. Owing to weaker interactions between solvated ions in the ion-pairs, the ion pairing process will be less affected by temperature variations. Thus, fewer solvent molecules are released during the association process of LiTDI than during that of $LiPF_6$ and LiFSI.

4.5. Discussing the ion-pair structure of LiTDI, $LiPF_6$ and LiFSI in EC/DMC

Association of free ions into ion-pairs is an endothermic ($\Delta H^{\circ}_{IP} > 0$) and an exergonic ($\Delta G^{\circ}_{IP} < 0$) phenomenon for LiTDI, LiFSI and $LiPF_6$ in EC/DMC. Due to the nature of EC, a strongly polar molecule with a high dielectric constant preferentially solvating Li^+ in EC/DMC,[38] the formation of CIP is unlikely. This kind of ion-pairs are found in solvents of low dielectric constant like dioxanne, benzene or cyclohexane. A positive value for ΔH°_{IP} indicates that the desolvation, which occurs during the formation of the ion-pairs, brings a predominant positive contribution (ΔH_{sol}) to the standard enthalpy over the negative contribution due to the released coulombic energy (ΔH_{el}). Thus, the formation of a SIP structure appears more likely for $LiPF_6$ and LiFSI. Concerning LiTDI, for which the $\Delta H^{\circ}_{IP}(T)$ slop is weaker than that of LiFSI and $LiPF_6$, the modulus of the two different contributions of the association enthalpy might be close enough to nearly compensate each other which is in fair agreement with a S_2IP type of ion-pairing as stated previously.

It was also noticed that the average Li^+ effective solute radius, which takes into account free solvated lithium ions and those engaged in IP or larger aggregates, could vary with the temperature. A reduction of this radius after a rise in temperature (LiFSI) would suggest the formation of ion-pairs of the SIP type. On the contrary, an increase or no variation of the effective solute radius with the temperature (LiTDI) would more likely suggest the formation of S_2IP.

Finally, $LiPF_6$ presents a peculiar behavior. The Li^+ effective solute radius increases with the temperature and, it is the only salt that exhibits a negative standard enthalpy at room temperature or below. As the number of free ions within the solution decreases when the temperature is raised, this phenomenon can be explained by the transformation of a number of SIP into S_2IP. This also explains the change in sign of ΔH°_{IP} for $LiPF_6$-based electrolyte in EC/DMC.

5. Conclusion

The conductivity and viscosity study of LiFSI, LiTDI and $LiPF_6$ solutions in EC/DMC show that these two transport processes are not strictly coupled as their activation energies differ by 1 to 2 kJ mol^{-1}. The reason for that could be the formation of ion-pairs when the concentration in salt in solution is increased to 1 mol L^{-1}. The best conductivity at room temperatures is obtained for LiFSI followed closely by $LiPF_6$, the reason for this being a lower dissociation coefficient for LiTDI. In addition, the maximum in conductivity is obtained in the case of LiFSI and $LiPF_6$ around 1 mol L^{-1} but only 0.75 mol L^{-1} for LiTDI.

The ion-pair dissociation coefficient (α_D) and the lithium cation effective solute radius (r_s) of the LiTDI, LiFSI and $LiPF_6$ salts in an EC/DMC binary solvent were investigated at temperatures ranging from 25 °C to 80 °C. The ion-pair structures of these salts, *i.e.* solvent-shared ion-pair (SIP) and solvent separated ion-pair (S_2IP), were deduced from the study of the variations of α_D and r_s. α_D was determined by using the Walden rule and also by using the self-diffusion coefficients values and the Nernst–Einstein equation. Both methods gave results in fair agreement for the variations of α_D with the temperature. In a similar way, r_s was calculated using the Jones–Dole–Kaminsky equation coupled with the Einstein relation and the Stokes–Einstein equation. Even though the first method leads to higher values for r_s than the other, there was a good agreement concerning the variations of r_s with the temperature. By analyzing the variations of α_D and r_s with the temperature, LiFSI and $LiPF_6$

Open Access Article. Published on 06 febrero 2019. Downloaded on 14/08/2025 20:05:26.
This article is licensed under a Creative Commons Attribution-NonCommercial 3.0 Unported Licence.

ion-pairs could be characterized as SIP. However, in the case of $LiPF_6$ ΔH°_{IP} exhibits a sign change above room temperature meaning that SIP and S_2IP could co-exist at room temperature and that a number of SIP transform to S_2IP when the solution temperature is raised. In the case of the LiTDI-based electrolyte, α_D, $r_{s,}$ ΔH°_{IP} and ΔS°_{IP} are not temperature dependent. This has been assigned to the fact that LiTDI ion-pairs are of the S_2IP type.

The temperature dependence of the Gibbs free energy, enthalpy and entropy for the ion-association process thermodynamic parameters allowed us to confirm the selected ion-pair structure for each lithium salt. Moreover, the standard Gibbs free energy ΔG°_{IP} for ion-pair formation is negative for all electrolytes meaning that this process is exergonic. ΔS°_{IP} is positive at all temperature investigated indicating that there is a net increase in the number of free solvent molecules during the ion association process. ΔH°_{IP} is positive excepted for $LiPF_6$ at room temperature or below. It can be concluded that the desolvation process is more energetic than the coulombic contribution to the overall ion-pair formation. Future work will now be devoted to Raman spectroscopy in order to confirm the ion-pair structures.

Conflicts of interest

There are no conflicts to declare.

References

1 J. M. Tarascon and M. Armand, *Nature*, 2001, **414**, 359–367.
2 M. Armand and J. M. Tarascon, *Nature*, 2008, **451**, 652–657.
3 B. Scrosati and J. Garche, *J. Power Sources*, 2010, **195**, 2419–2430.
4 E. M. Erickson, C. Ghanty and D. Aurbach, *J. Phys. Chem. Lett.*, 2014, **5**, 3313–3324.
5 D. Linden, *Handbook of Batteries*, 3rd ednn, McGraw-Hill, 2002.
6 A. Yoshino, *Angew. Chem., Int. Ed.*, 2012, **51**, 5798–5800.
7 Y. Nishi, H. Azuma and A. Omaru, *US Pat.*, No. 4 959 281, 1990.
8 H. U. Sverdrup, *Resour., Conserv. Recycl.*, 2016, **114**, 112–129.
9 Y. Yang, M. T. McDowell, A. Jackson, J. J. Cha, S. S. Hong and Y. Cui, *Nano Lett.*, 2010, **10**, 1486–1491.
10 B. L. Ellis, K. T. Lee and L. F. Nazar, *Chem. Mater.*, 2010, **22**, 691–714.
11 R. Petibon, V. L. Chevrier, C. P. Aiken, D. S. Hall, S. R. Hyatt, R. Shunmugasundaram and J. R. Dahn, *J. Electrochem. Soc.*, 2016, **163**, A1146–A1156.
12 N. Liu, H. Wu, M. T. McDowell, Y. Yao, C. Wang and Y. Cui, *Nano Lett.*, 2012, **12**, 3315–3321.
13 T. Li, Y. L. Cao, X. P. Ai and H. X. Yang, *J. Power Sources*, 2008, **184**, 473–476.
14 M. Sanders, *Lithium-Ion Battery Raw Material & Demand 2016-2025*, San Francisco, CA, 2017.
15 L. Li, S. Zhou, H. Han, H. Li, J. Nie, M. Armand, Z. Zhou and X. Huang, *J. Electrochem. Soc.*, 2011, **158**, A74.
16 A. Borun and A. Bald, *J. Chem. Eng. Data*, 2016, **61**, 3788–3793.
17 M. Bachelin, P. Gans and J. B. Gill, *J. Chem. Soc., Faraday Trans.*, 1992, **88**, 3327–3330.
18 P. Gans, J. B. Gill and P. J. Longdon, *J. Chem. Soc., Faraday Trans. 1*, 1989, **85**, 1835–1839.
19 D. G. Thomas, *J. Colloid Sci.*, 1965, **20**, 267–277.
20 G. Jones and M. Dole, *J. Am. Chem. Soc.*, 1929, **51**, 2950–2964.
21 M. Kaminsky, *Z. Phys. Chem.*, 1957, **12**, 206.
22 K. G. Lawrence, A. Sacco, A. De Giglio and A. Dell'Atti, *J. Chem. Soc., Faraday Trans. 1*, 1989, **85**, 23–32.
23 N. Martinus, D. Crawford, D. Sinclair and C. A. Vincent, *Electrochim. Acta*, 1977, **22**, 1183–1187.
24 A. A. M. M. Lencka, S. J. Sanders and R. D. Young, *Int. J. Thermophys.*, 1998, **19**.
25 P. Z. Walden, *Physik Chem.*, 1906, **55**, 207–246.
26 *A Dictionary of Chemistry*, ed. J. Daintith, Oxford University Press, 6th edn, 2008, Print ISBN-13: 9780199204632, DOI: 10.1093/acref/9780199204632.001.0001.
27 W. Xu, E. I. Cooper and C. A. Angell, *J. Phys. Chem. B*, 2003, **107**, 6170–6178.
28 C. Austen Angell, Y. Ansari and Z. Zhao, *Faraday Discuss.*, 2012, **154**, 9–27.
29 C. A. Angell, *Solid State Ionics*, 1983, **9**, 3–16.
30 M. P. Longinotti and H. R. Corti, *J. Phys. Chem. B*, 2009, **113**, 5500–5507.
31 W. X. Masahiro Yoshizawa and C. Austen Angell, *J. Am. Chem. Soc.*, 2003, **125**, 15411–15419.
32 C. L. Berhaut, P. Porion, L. Timperman, G. Schmidt, D. Lemordant and M. Anouti, *Electrochim. Acta*, 2015, **180**, 778–787.
33 A. Ferry, G. Orädd and P. Jacobsson, *Electrochim. Acta*, 1998, **43**, 1471–1476.
34 M. P. Longinotti and H. R. Corti, *J. Phys. Chem. B*, 2009, **113**, 5500–5507.
35 C. Schreiner, S. Zugmann, R. Hartl and H. J. Gores, *J. Chem. Eng. Data*, 2009, **55**, 1784–1788.
36 Y. Aihara, K. Sugimoto, W. S. Price and K. Hayamizu, *J. Chem. Phys.*, 2000, **113**, 1981–1991.
37 L. Niedzicki, S. Grugeon, S. Laruelle, P. Judeinstein, M. Bukowska, J. Prejzner, P. Szczeciński, W. Wieczorek and M. Armand, *J. Power Sources*, 2011, **196**, 8696–8700.
38 K. Xu and A. Von Cresce, *ECS Trans.*, 2012, **41**, 187–193.

This journal is © The Royal Society of Chemistry 2019